The Astrophysical Journal, 846:27 (14pp), 2017 September 1 https://doi.org/10.3847/1538-4357/aa8322
© 2017. The American Astronomical Society. All rights reserved.

GASP. IV. A Muse View of Extreme Ram-pressure-stripping in the Plane of the Sky: The Case of Jellyfish Galaxy JO204

Marco Gullieuszik[1], Bianca M. Poggianti[1], Alessia Moretti[1], Jacopo Fritz[2], Yara L. Jaffé[3], George Hau[3], Jan C. Bischko[4], Callum Bellhouse[3], Daniela Bettoni[1], Giovanni Fasano[1], Benedetta Vulcani[1,5], Mauro D'Onofrio[6], and Andrea Biviano[7]
[1] INAF—Astronomical Observatory of Padova, vicolo dell'Osservatorio 5, I-35122 Padova, Italy; marco.gullieuszik@oapd.inaf.it
[2] Instituto de Radioastronomía y Astrofísica, IRyA, UNAM, Campus Morelia, A.P. 3-72, C.P. 58089, Mexico
[3] European Southern Observatory, Alonso de Córdova 3107, Santiago, Chile
[4] Institute of Astro- and Particle Physics, University of Innsbruck, Technikerstrasse 25, A-6020 Innsbruck, Austria
[5] School of Physics, University of Melbourne, VIC 3010, Australia
[6] Department of Physics and Astronomy, University of Padova, Vicolo Osservatorio 3, I-35122 Padova, Italy
[7] INAF–Astronomical Observatory of Trieste, via G.B. Tiepolo 11, I-34131 Trieste, Italy
Received 2017 May 4; revised 2017 July 7; accepted 2017 July 17; published 2017 August 29

Abstract

In the context of the GAs Stripping Phenomena in galaxies with Muse (GASP) survey, we present the characterization of JO204, a jellyfish galaxy in A957, a relatively low-mass cluster with $M = 4.4 \times 10^{14}\,M_{\odot}$. This galaxy shows a tail of ionized gas that extends up to 30 kpc from the main body in the opposite direction of the cluster center. No gas emission is detected in the galaxy outer disk, suggesting that gas-stripping is proceeding outside-in. The stellar component is distributed as a regular disk galaxy; the stellar kinematics shows a symmetric rotation curve with a maximum radial velocity of 200 km s^{-1} out to 20 kpc from the galaxy center. The radial velocity of the gas component in the central part of the disk follows the distribution of the stellar component; the gas kinematics in the tail retains the rotation of the galaxy disk, indicating that JO204 is moving at high speed in the intracluster medium. Both the emission and radial-velocity maps of the gas and stellar components indicate ram-pressure as the most likely primary mechanism for gas-stripping, as expected given that JO204 is close to the cluster center and it is likely at the first infall in the cluster. The spatially resolved star formation history of JO204 provides evidence that the onset of ram-pressure-stripping occurred in the last 500 Myr, quenching the star formation activity in the outer disk, where the gas has been already completely stripped. Our conclusions are supported by a set of hydrodynamic simulations.

Key words: galaxies: clusters: general – galaxies: evolution – galaxies: general – galaxies: kinematics and dynamics – intergalactic medium

1. Introduction

The evolution of galaxies is primarily regulated by the processes of gas inflow and outflow. A galaxy without a reservoir of gas will soon stop its star formation activity and will therefore evolve into a red and passive galaxy. Peng et al. (2010) showed that the differential effects of galactic mass and of the environment in the quenching of galaxies are fully separable, and introduced the idea of two distinct processes operating: "mass quenching" and "environment quenching."

The evolution of isolated galaxies is mainly driven by the balance of gas consumption by star formation, gas-loss by outflows, and gas accretion. The main driver for these processes is the galaxy mass; in general, massive galaxies are more likely to consume all the gas reservoir and become quiescent than low-mass galaxies. The most direct evidence of the environment effect in quenching the star formation history is the morphology–density relation (Dressler 1980; Fasano et al. 2015): the fraction of late-type galaxies decreases from ∼80% in the field to ∼60% in the outskirts of galaxy clusters to virtually zero in the cores of rich clusters.

Gravitational interactions are obvious candidate mechanisms that could efficiently remove the gas from galaxies; these include strong tidal interactions and mergers between galaxies (Barnes & Hernquist 1992), tidal interactions with the cluster potential (Byrd & Valtonen 1990), and so-called harassment, which is the effect of multiple high-speed galaxy–galaxy close encounters (Moore et al. 1996). Another class of possible quenching mechanisms is the interactions of the cold disk gas with the hot intracluster medium (ICM), like thermal evaporation (Cowie & Songaila 1977), viscous stripping (Nulsen 1982), or ram-pressure stripping (Gunn & Gott 1972). Moreover, further infall of gas into the galaxy disk can be prevented by the removal of the outer galaxy gas halo (by either hydrodynamic interaction with the ICM or tidal forces), thus causing quenching by starvation (Larson et al. 1980).

In galaxy clusters, ram-pressure-stripping is expected to be the most efficient of the aforementioned processes. In the inner regions of rich clusters, galaxy–galaxy interactions are expected to be inefficient and rare because of the large velocity dispersion; for the same reason, and because of the high density of the ICM, this environment is instead considered highly favorable for ram-pressure-stripping (e.g., Steinhauser et al. 2016). A clear observational signature of ongoing ram-pressure stripping is an uneven gas distribution in the galaxy disk (Giovanelli & Haynes 1985; Gavazzi 1989). In the most extreme cases, extended one-sided gas tails of gas can be observed to extend up to many disk scale-lengths: these spectacular examples of gas-stripping galaxies are commonly referred to as jellyfish galaxies (Cortese et al. 2007; Smith et al. 2010; Owers et al. 2012; Ebeling et al. 2014). The first systematic searches of jellyfish galaxies were conducted recently in nearby (Poggianti et al. 2016) and high-redshift

($z = 0.3$–0.7) clusters (Ebeling et al. 2014; McPartland et al. 2016).

GASP[8] (GAs Stripping Phenomena in galaxies with MUSE) is an ESO Large program aimed at studying where, how, and why gas can be removed from galaxies. GASP targets 94 candidate stripping galaxies selected from the Poggianti et al. (2016) catalog, which was built on a systematic search for galaxies with signatures of one-sided debris or tails reminiscent of gas-stripping processes in optical images of clusters from WINGS (Fasano et al. 2006) and OmegaWINGS (Gullieuszik et al. 2015) surveys and groups from the Padova Millennium Galaxy and Group Catalog (PM2GC, Calvi et al. 2011). GASP was granted 120 hr of observing time with the integral-field spectrograph MUSE mounted at the VLT; observations started in 2015 October and—at the current rate of execution—we foresee the end of GASP observations by the end of 2018. A complete description of the survey strategy, data reduction, and analysis procedures is presented in Poggianti et al. (2017b).

In this paper we present GASP observations of the galaxy JO204 in Poggianti et al. (2016), which is J101346.82–005450.9 in the WINGS database (Moretti et al. 2014). This galaxy turned out to be one of the most spectacular cases of jellyfish galaxies observed by GASP to date. The paper is organized as follows. In Section 2 we present GASP observations and data reduction; in Section 3 we describe the data analysis; Section 4 describes JO204's environment; in Section 5 we present a set of hydrodynamic simulations of ram-pressure-stripping in a galaxy resembling JO204; and in Section 6 we summarize the paper and provide our main conclusions.

In this paper we adopt a Chabrier (2003) IMF and standard concordance cosmology with $H_0 = 70$ km s^{-1} Mpc^{-1}, $\Omega_M = 0.3$, $\Omega_\Lambda = 0.7$. This gives a scale of 0.887 kpc/arcsec at the redshift of A957, that is $z = 0.0451$ (Moretti et al. 2017).

2. Observations and Data Reduction

All GASP observations are carried out in service mode with the MUSE spectrograph (Bacon et al. 2010), mounted at the Nasmyth focus of the UT4 VLT, at Cerro Paranal in Chile. MUSE is composed of 24 IFU modules and each of them is equipped with a 4k × 4k CCD. The spectral range, between 4500 and 9300 Å, is sampled at 1.25 Å/pixel, with a spectral resolution of ∼2.6 Å. The resolving power at 7000 Å is $R = 2700$, corresponding to 110 km s^{-1} or 53 km s^{-1} pixel^{-1}. The $1' \times 1'$ field of view is sampled at $0\farcs2$/pixel; each datacube therefore consists of $\sim 10^5$ spectra.

JO204 is a member of the Abell 957 (A957) cluster and is located $2\farcm1$ from the cluster center (see Figure 1), which corresponds to a projected distance of 132 kpc. JO204 hosts a known AGN (J101346.8–005451, Véron-Cetty & Véron 2010) with a double-peaked [O III] (Wang et al. 2009); this feature is interpreted as either a binary AGN or a sign of an outflow (see, e.g., Müller-Sánchez et al. 2015). JO204 was classified as a very probable jellyfish galaxy (JClass = 5) because in WINGS *B*-band images it shows a unilaterally disturbed morphology, with filaments suggesting ongoing ram-pressure gas-stripping (see Figure 2).

For JO204 we adopted an observing strategy slightly different from the standard GASP one (Poggianti et al. 2017b). Observations were split into three blocks, each consisting of two 675 s exposures. The pointing of each block was shifted in the northeast direction to extend the coverage of the JO204 gas tail (see Figure 2). Observations were carried out on three different nights—2015 December 05, 2016 January 06, and 2016 February 27—under good weather conditions (the ESO DIMM recorded a seeing between $0\farcs7$ and $1\farcs0$). Raw data were reduced using the latest ESO MUSE pipeline available after the observations were completed (v1.2.1)[9], following the standard GASP data reduction procedure, which is described in detail in Poggianti et al. (2017b).

The final stacked MUSE datacube consists of 353 × 369 sky-subtracted, flux-calibrated spectra with radial velocities corrected to the barycenter of the solar system. The FWHM of point-like sources on the image, obtained by convolving the final MUSE datacube with the *V*-band filter, is $0\farcs8$ (4 pixels).

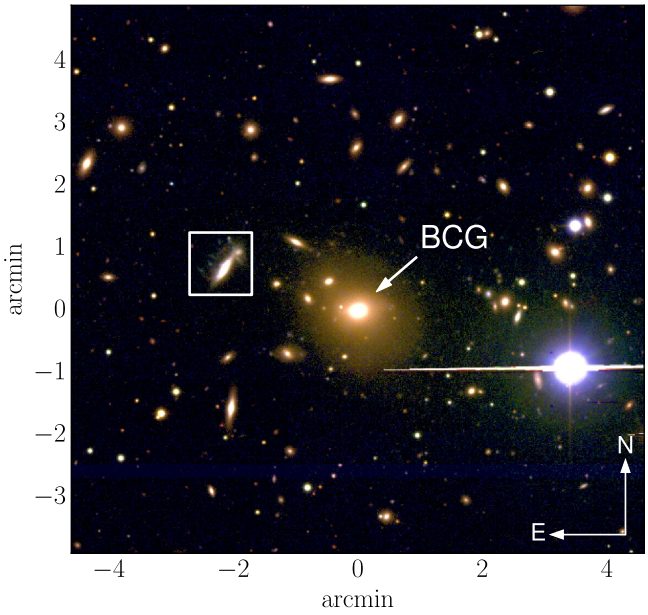

Figure 1. RGB image of the central region of A957 obtained from OmegaWINGS *u*- and WINGS *B*- and *V*-band images. The footprint of the field observed by MUSE is shown by the white box. The position of the brightest cluster galaxy is marked by the arrow.

3. Analysis

MUSE observations reveal that the faint extraplanar emission visible in optical broadband images (upper panel in Figure 2) is actually an extended tail of ionized gas, with strong Hα emission. This is evident from the RGB image obtained from the MUSE datacube that is shown in the lower panel of Figure 2. The blue and the green channels were obtained by integrating the MUSE datacube over a band of ±20 Å centered on the wavelength of [O III]5007 and Hα (rest-frame); for the red channel we selected a band with no emission lines from JO204, from 7100 to 7200 Å. We selected the brightest pixel in this red image as the center of JO204 and we defined it as the origin of the spatial coordinate system for all maps presented in this paper.

JO204 shows extended regions of Hα emission (green in Figure 2), out to ∼30″–40″ (∼30 kpc) from the disk. In the filaments of diffuse Hα emission there are many compact

[8] http://web.oapd.inaf.it/gasp

[9] The quality of the pipeline products fulfills the scientific requirements of the GASP survey; thus we decided not to reprocess all raw data with a more recent version of the software.

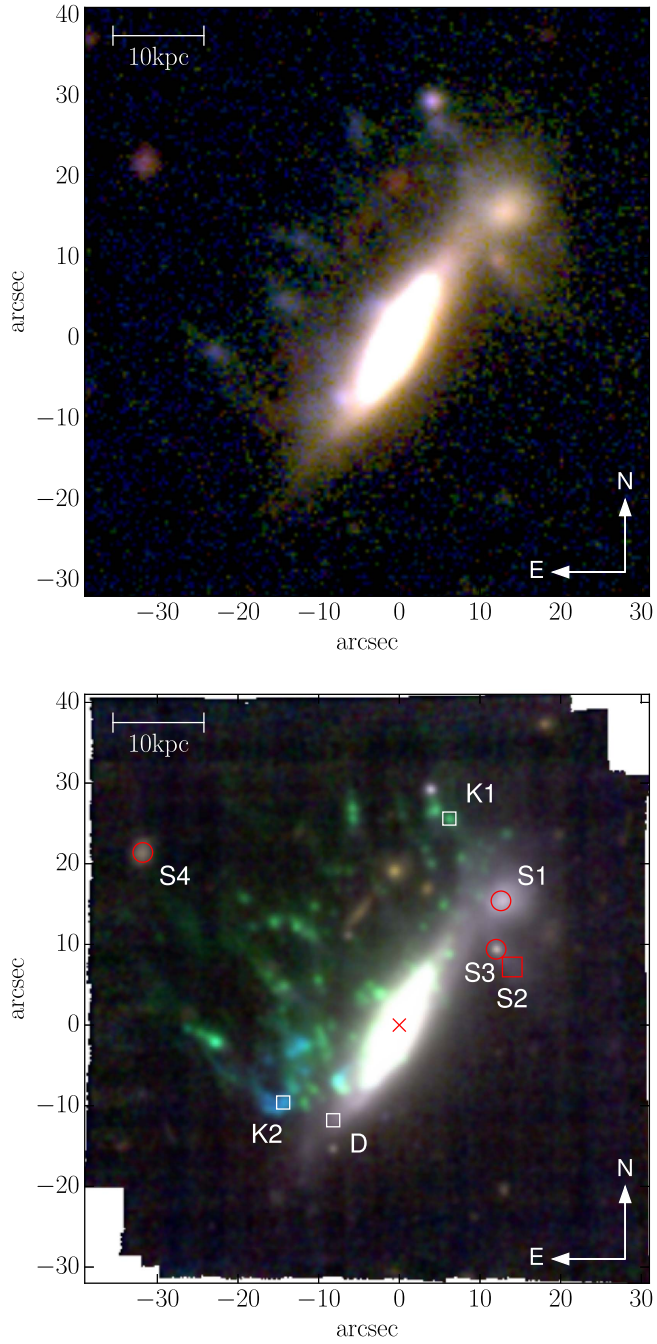

Figure 2. Upper panel: zoom-in of the image in Figure 1 on JO204. Lower panel: RGB color image of JO204 obtained using [O III]5007 for the blue channel, Hα for the green one, and the continuum from 7100 and 7200 Å for the red one. The sources marked by squares and circles are discussed in the text. The cross is the optical center, which was defined as the origin of the coordinate systems of all maps in this paper. Areas in white are not covered by MUSE data; in the upper right and lower left corners one can see the effect of the offset applied to the pointing center of the three observing blocks.

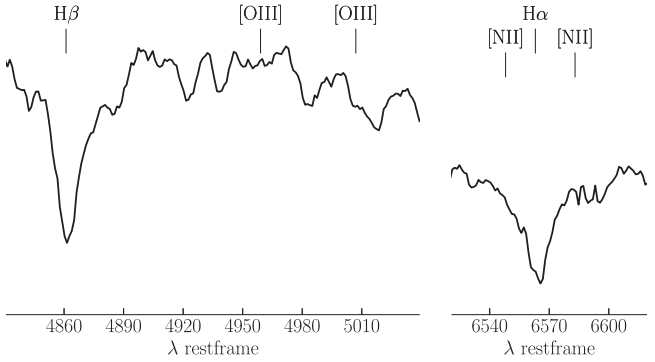

Figure 3. The k+a post-starburst spectrum (on an arbitrary scale) of a 1″ region in the outer disk of JO204 (region D in Figure 2).

emitting knots (an example is the one labeled K1 in Figure 2), which are shown to be active star-forming H II regions later in this paper. In the east part of the tail, approximately at (−10″, −15″) from the center of the galaxy, there is an extended region with a prominent [O III] emission, including an extremely bright compact region, labeled K2 in Figure 2. The differences in [O III]/Hα flux ratios across JO204 strongly suggest that different ionizing mechanisms are at work. The ionized gas emission will be further discussed in Section 3.4.

In the outer southeast side of the disk—which is visible out to ∼(−15″, −10″)—there is no gas emission, as demonstrated by the spectrum shown in Figure 3, which was obtained by integrating the MUSE datacube over a 1″ region at ∼−8′, −12′ from the center (marked as D in Figure 2). This spectrum shows a steep blue stellar continuum and strong Balmer absorptions (EW(Hβ) = 6.1 Å and EW(Hα) = 3.4 Å (rest-frame)); these features are typical of young post-starburst stellar populations with strong star formation activity rapidly quenched in the last Gyr (Couch & Sharples 1987; Poggianti et al. 1999).

In addition to JO204, other sources are detected in the MUSE datacube; we characterized all of them to assess any possible contamination in the analysis of JO204. Some of these sources are marked in Figure 2. The object marked as S1 is a galaxy at $z \simeq 0.052$ with a typical post-starburst spectrum; the Hβ equivalent width measured by integrating the spectrum on a circular region of 1″ is EW(Hβ) = 8.6 Å (rest-frame) in absorption. The spectrum of the diffuse object region around S2 shows no emission lines and weak Balmer lines in absorption at a redshift similar to that of S1; this is most likely a passive galaxy member of A957 cluster. S3 is a Milky Way star. The spectra of these three sources show no emission lines, and therefore they do not affect the analysis of JO204 gas emission. However, the absorption features of S1, S2, and S3 could potentially affect the analysis of the stellar component of JO204, therefore we masked out the regions around these three sources for the analysis of the JO204 stellar component (see Section 3.1). S4 is a star-forming galaxy at $z \simeq 0.36$. The strong [O III]5007 emission line of this galaxy is redshifted at a wavelength not far from the expected location of Hα emission of JO204. We visually inspected the MUSE datacube and found no signal of any possible emission from JO204 around S4; however, to avoid any possible confusion in the analysis, we masked out a region of 5″ around S4. A few background galaxies are also visible in Figure 2. These sources do not significantly affect any feature in the spectrum of JO204 or its tail.

The observed datacube was corrected for Galactic extinction adopting a value $E_{B-V} = 0.037$ extracted from Schlafly & Finkbeiner (2011) reddening maps and the Cardelli et al. (1989) extinction law. In this paper we are mostly interested in

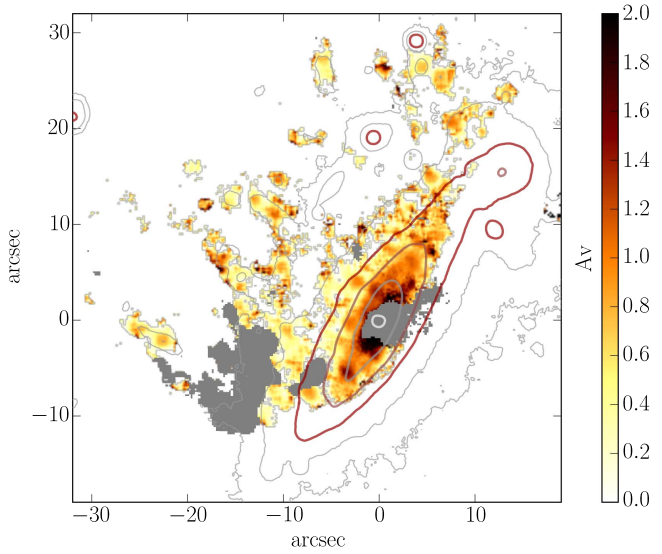

Figure 4. Extinction map by dust internal to JO204. A_V is estimated assuming that the gas is ionized by young stars, therefore the values obtained for regions ionized by shocks (AGNs/LINERs) could not be reliable. These regions (see Section 3.4) are shaded in gray. Isophotes of Hα continuum in steps of 0.5 mag/arcsec^{-2} are shown to trace the stellar emission.

the low-surface brightness emission from the diffuse gas in the tail; therefore, to increase the signal-to-noise ratio (S/N), we applied a 5-pixel-wide boxcar filter to the datacube; this means that each spaxel (at each wavelength), was replaced with the average value of the 5×5 neighboring spaxels. This procedure does not significantly alter the spatial resolution of the data, as the filter size is similar to the seeing (0.″8, see Section 2) and it conserves the total flux. A first estimate of the emission line fluxes and gas radial-velocity map was extracted from the resulting smoothed extinction-corrected datacubes; with this purpose we fit a combination of 1D Gaussian functions to the Hβ, [O III]4959, [O III]5007, [O I]6300, Hα, [N II]6548, [N II]6583 and [S II]6716, and [S II]6731 lines using the KUBEVIZ (Fossati et al. 2016) software.

KUBEVIZ also outputs the continuum level for each line; when no Hα emission is detected, this value simply corresponds to the mean value of the continuum in the Hα spectral region (at the redshift of JO204). To trace the distribution of the stellar component, we extracted from the Hα-continuum map contour lines (in steps of 0.5 mag arcsec^{-2}). The resulting isophotes are shown in Figure 4 and most of the maps in this paper.[10]

The spectrum of the central region of JO204 in Figure 6 shows a blue wing in the [O III] lines; a visual inspection of the datacube confirms the presence of more than one gas component in the central region ($\sim$5 kpc) of JO204, likely due to the AGN outflows. Besides the central regions, however, the line profiles are well described by a single component and therefore we will base the analysis of this paper on the simple single-component fit results. The presence of multiple gas component in the central regions of JO204 does not affect any of the main conclusions of this paper, which is mainly focused on the properties of the stripped gas. An analysis of the central active region of JO204 and other GASP galaxies using a multi-component fit to MUSE spectra is presented in Poggianti et al. (2017a).

3.1. Modeling the Stellar Component

For the whole sample of galaxies in the GASP survey it is of primary importance to disentangle the gas and the stellar components in the observed spectra. The stellar component is analyzed by masking out the spectral regions of the principal emission lines. As a first step, we performed an adaptive spatial binning of the MUSE datacube using the Voronoi tessellation method of Cappellari & Copin (2003), requiring a minimum S/N of 10 on each binned region. As discussed in the previous section, we masked out the regions around S1, S2, and S3 (see Figure 2). The stellar radial velocity for each Voronoi bin was then computed with the pPXF code (Cappellari & Emsellem 2004). The resulting stellar velocity map is presented and discussed in Section 3.3.

The spatially resolved properties of the stellar populations were obtained using the spectral fitting code SINOPSIS (Fritz et al. 2017) as described in Poggianti et al. (2017b). This code combines different single-stellar-population spectra to reproduce the observed equivalent widths of the main absorption and emission lines, as well as the continuum in various wavelength bands. The outputs of SINOPSIS are maps of: (i) stellar mass; (ii) average star formation rate (SFR) and total mass formed in four age bins[11]; and (iii) luminosity-weighted and mass-weighted stellar ages. In addition, it produces a best-fit model datacube for the stellar-only component. The derivation of the SFR as a function of the cosmic time from optical spectra is both model-dependent and prone to uncertainties, mainly due to the parameters' degeneracy, which is intrinsic to the problem. The ability and the limitations of SINOPSIS in recovering the SFH have been extensively tested by Fritz et al. (2007, 2011) using both mock and real data. The choice of the four age bins was done based both on the results of this comparison, and on the differences between the spectral features of simple stellar population spectra as a function of age. When applied to spatially resolved data like these the method has proved to be even less prone to uncertainties, as highlighted in Fritz et al. (2017).

3.2. Emission-only Datacubes

The spectra of the gas component were obtained by subtracting the best-fit stellar model obtained with SINOPSIS to the extinction-corrected datacube. We run KUBEVIZ on the resulting emission-only datacube to refine the gas radial-velocity maps and obtain the corrected emission fluxes for all emission lines. The measured fluxes were then corrected for extinction by dust internal to JO204. The correction was carried out assuming an intrinsic Hα/Hβ = 2.86 and the Cardelli et al. (1989) extinction law. Figure 4 shows that the highest values of the extinction in JO204 are found at the center ($A_V \gtrsim 2$ mag); we found values around $A_V \sim 1.0$ mag on the galaxy disk, out to $\sim$10″. The extraplanar dust in the gas tail has a clumpy distribution, with compact regions with $A_V \sim 1.0$ mag; outside these dust-rich knots the extinction is generally lower, with $A_V \lesssim 0.5$ mag. In the following sections we will show that the high-extinction regions are bright compact sources of Hα emission, as usually seen for star-forming H II regions.

[10] The isophotes also trace the continuum emission from interlopers, such as S1, S2, S3, and S4 (see Figure 2).

[11] Young: $<2 \times 10^7$ yr; recent: [2×10^7 yr, 5.7×10^8 yr]; intermediate-age [5.7×10^8 yr; 5.7×10^9 yr]; and old: $>5.7 \times 10^9$ yr.

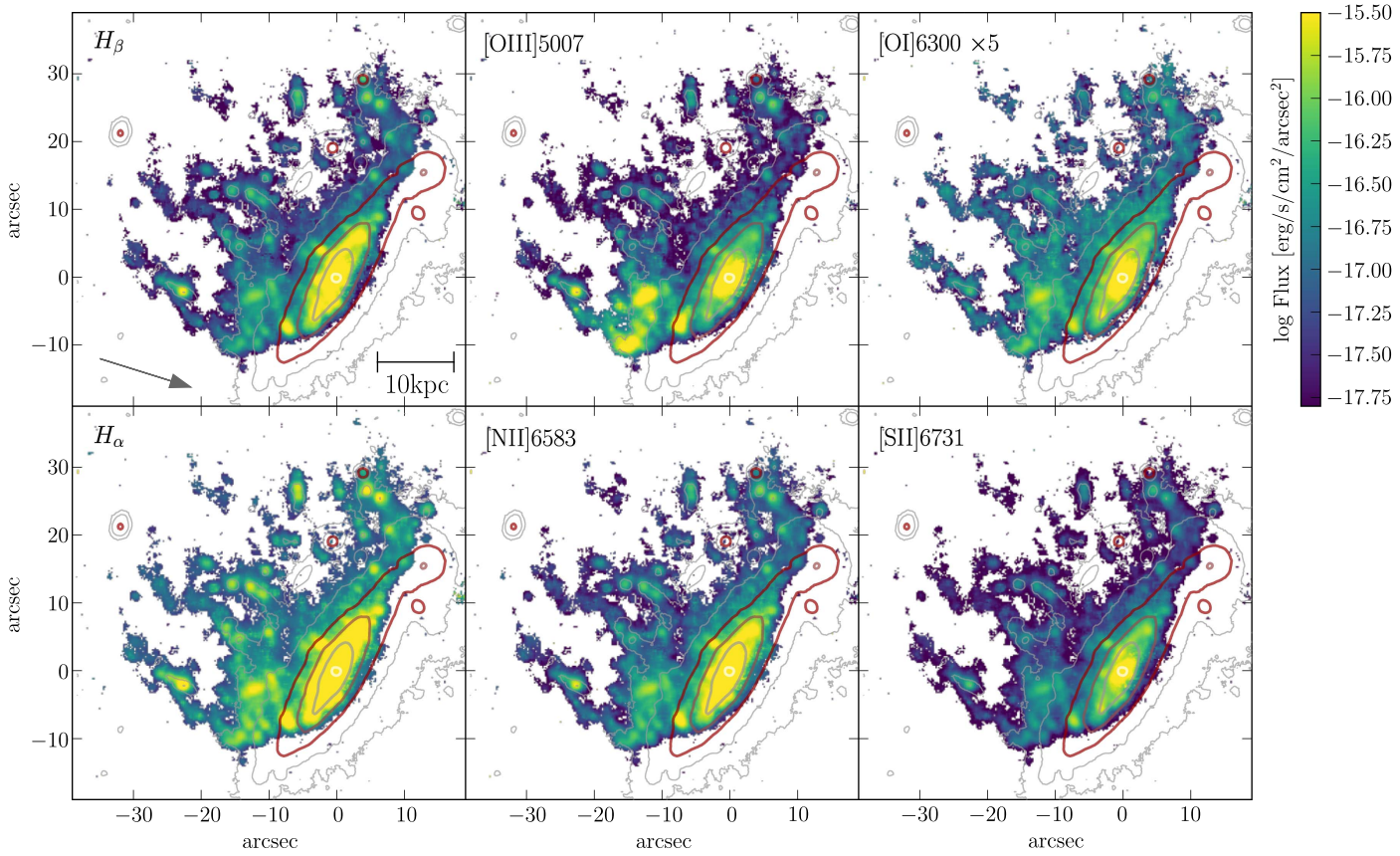

Figure 5. Absorption-corrected flux emission maps of the principal emission lines. The [O I] line is on average weaker than the others; to enhance the faint structures and keep the same scale for all maps, [O I] is displayed multiplied by a factor 5. Only spaxels with S/N of Hα flux >5 are shown. Hα continuum isophotes are the same as in Figure 4. The arrow in the upper left panel points to the cluster center.

The maps of the dust-corrected emission-only fluxes for the principal emission lines are shown in Figure 5, masking all spaxels where the S/N of the Hα flux is less than 5. The flux maps obtained for JO204 confirm the extraordinary sensitivity of MUSE, which allows detection of faint sources, down to $F_{\rm H\alpha} \simeq 10^{-17.5}$ erg s^{-1} cm^{-2} arcsec^{-2} with an S/N = 5. This value is the typical detection limit of the GASP survey (Poggianti et al. 2017b) and is similar to the one obtained by other MUSE observations (Fumagalli et al. 2014; Fossati et al. 2016).

The emission line maps in Figure 5 clearly unveil the bright tail of ionized gas in JO204. This tail is developed along a direction perpendicular to the JO204 disk and is populated by a large number of compact knots with strong Balmer-line emission. The strong [O III] emission region around K2 (see Figure 2) is clearly visible in Figure 5; the spectrum of K2 is shown together with those of K1 and the JO204 center in Figure 6; the spectra in the central region of the galaxy have emission lines with dispersion ∼300 km s^{-1} and [O III]/Hβ and [N II]/Hα line ratios typical of AGN emission; the line ratios in the K2 spectrum have similar characteristics, while K1 shows features typical of photoionized star-forming H II regions. The characterization of the ionizing mechanisms of the gas component in JO204 is presented in Section 3.4.

The stellar disk, traced by the continuum isophotes in Figure 5, extends at least up to ∼30″ from the center. In the outer part of the disk there is no evidence of any emission from the gas component, which is detected along the JO204 major axis only in the inner 10″.

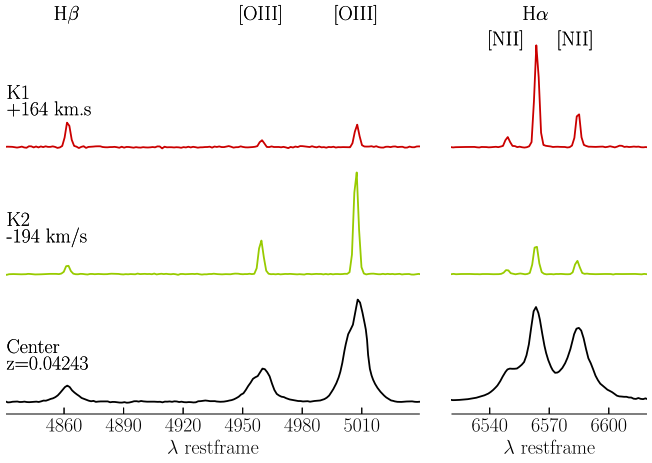

Figure 6. Pure emission spectra of the center of JO204 and of regions K1 and K2 (see Figure 2). Spectra were obtained by subtracting the stellar component from the observed spectra. The spectra of the center of JO204 and K2 are typical of regions ionized by AGN activity (strong [O III] and [N II]), while the K1 emission is typical of star-forming clumps.

3.3. Gas and Stellar Kinematics

The velocity map of the gas and stellar components of JO204 is shown in the upper panel of Figure 7. Radial velocities are referred to as the value obtained for the stellar component at the center of the galaxy, which is $z = 0.04243$. The value of the stellar radial velocity measured by pPXF in each Voronoi bin

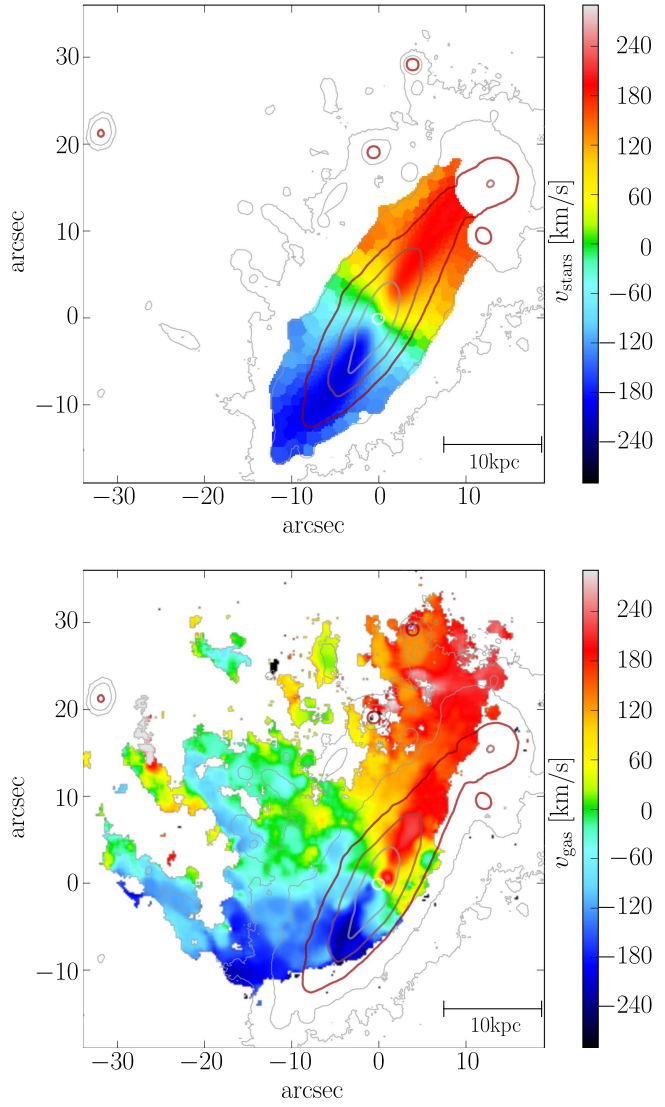

Figure 7. Velocity map of the JO204 stellar component (upper panel) and gas (lower panel). The Hα-continuum isophotes are the same as in Figure 4.

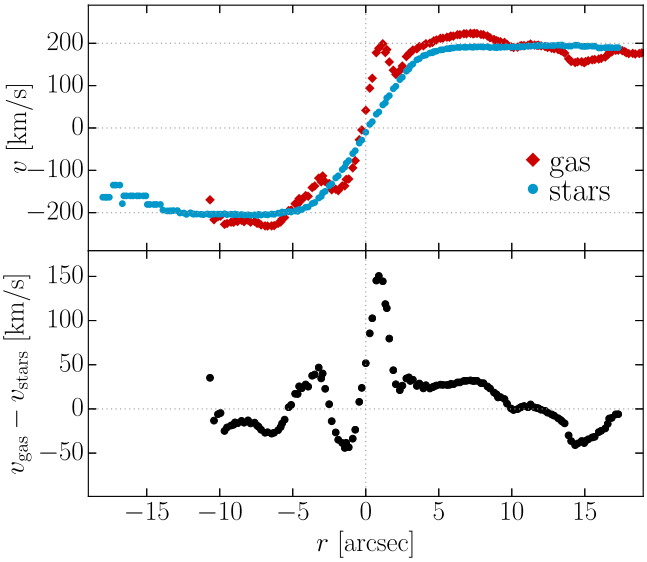

Figure 8. The upper panel shows the radial velocity for the gas and stellar component obtained along a slit aligned with the major axis of JO204. The difference between the radial velocities of the two components is shown in the lower panel.

was smoothed using the two-dimensional local regression techniques (LOESS) as implemented in the Python code developed by M. Cappellari.[12]

The radial-velocity distribution of the stellar component of JO204 is symmetric and it indicates a regular disk rotation. The maximum projected rotation velocity is $\sim\pm200$ km s^{-1} out to $\sim15''$–$20''$ (13–18 kpc). The regular rotation, together with the regular morphology of the stellar isophotes, confirms that the mechanism stripping the gas does not affect the stellar component, as expected for ram-pressure-stripping from the ICM. The Hα velocity map (lower panel of Figure 7) shows that, on the galaxy disk, the gas kinematics follows the stellar kinematics. The most notable difference between the gas and stellar velocity maps is the compact region with $v_{gas} \sim 200$ km s^{-1} located $\sim1''$ northwest of the center, which will be discussed in the following paragraph. The kinematics of the gas tail follows the rotation of the stellar disk with only marginal local perturbations. This is also observed in other jellyfish galaxies (Fumagalli et al. 2014; Poggianti et al. 2017b) and it is interpreted as a consequence of the high speed of the galaxy in the ICM.

To further analyze the kinematics of the two components, we extracted the gas and stellar radial velocities along a narrow slit on the major axis of JO204; the position angle (−30°) was estimated by fitting an ellipse to the third brightest isophote in Figure 5. The resulting (projected) rotation curves are shown in Figure 8. The gas component displays a double-hump rotation curve; the local minimum and maximum are located $\sim\pm1''$ from the center of JO204. This could be the signature of a bar, or a gas outflow from the AGN. The general shapes of the two curves are similar, however, and show a maximum radial velocity of 200 km s^{-1}; to test the robustness of these results we performed a few tests, varying the angle of the slit used to trace the gas and stellar radial-velocity curves. The stellar and gas kinematics do not show significant variations in the inner ($\sim10''$) disk other than the two aforementioned humps. Lastly, we note that the symmetry of the radial-velocity curves shows that the rotation center (of both the stellar and the gas components) corresponds to the center of the galaxy, as defined by the emission peak.

3.4. Gas Ionization Mechanism

To investigate the physical mechanism responsible for the gas ionization we used the line-ratio diagnostic Baldwin–Phillips–Terlevich (BPT, Baldwin et al. 1981) diagrams. Such diagrams are commonly used to distinguish sources photo-ionized by hot young stars from those ionized by Low-Ionization Nuclear Emission-line Regions (LIINERs) or AGNs. We built two BPT diagrams using [O III]5007/Hβ versus [S II] 6717+6731/Hα[13] and [O III]5007/Hβ versus [N II]6583/Hα line ratios obtained for each MUSE spaxel with S/N > 3. Results are shown in Figure 9. Classification of star-forming/composite regions, LINERs, and AGNs was performed following the results of Kauffmann et al. (2003), Kewley et al. (2001, 2006), and Sharp & Bland-Hawthorn (2010). The center of JO204 is dominated by the AGN emission.

[12] http://www-astro.physics.ox.ac.uk/~mxc/software

[13] [S II] 6717+6731 is the sum of the fluxes of the two [S II] lines.

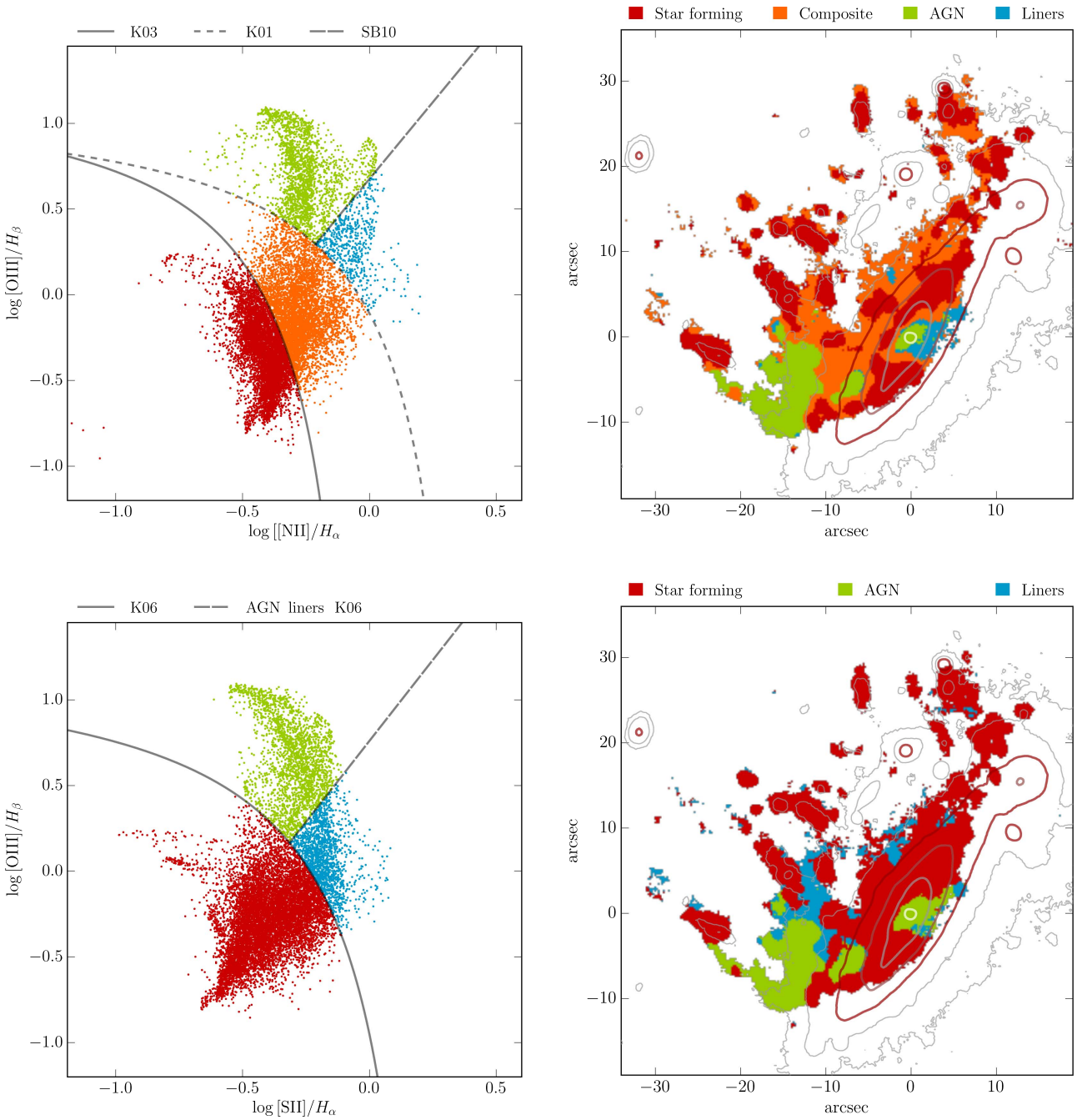

Figure 9. Left panels: BPT diagnostic diagrams for [O III]5007/Hβ vs. [N II]6583/Hα (top) and [O III]5007/Hβ vs. [S II]6717,6731/Hα (bottom) line ratios for all spaxels with fluxes measured with an S/N > 3. The lines used to separate star-forming (red dots), composite (orange), LINERs (blue), and AGNs (green) are from Kauffmann et al. (2003, K03), Kewley et al. (2001, K01), Kewley et al. (2006, K06), and Sharp & Bland-Hawthorn (2010, SB10), respectively. Right panels: corresponding maps showing the ionization mechanism as derived from the BTP diagrams. The contours are stellar isophotes, just as in Figure 4.

Interestingly, there is also an extended AGN-powered region 15–20 kpc away from the center; this is the bright [O III] region surrounding K2 in Figure 2 and it is likely an AGN ionization cone. The other side of the cone could be associated with the region that extends ∼5 kpc from the center in the opposite direction and is another region classified as a LINER or AGN-powered in the two BPT diagrams.

In addition to the center and the region being affected by the AGN-ionization cone, the gas in the disk and in the stripped tail is ionized by young stars. As noted by Poggianti et al. (2017b), these are very likely stars formed 10^7 year ago at most, within the stripped gas. Support for this hypothesis is given in Sections 3.6 and 3.7, where we show that the JO204 tail hosts many H II regions forming massive young stars that can ionize gas.

3.5. Metallicity

The gas metallicity and ionization parameter for each spaxel were calculated using the *pyqz* Python module[14] (Dopita et al. 2013) v0.8.2; the log(Q) and 12 + log(O/H) values are obtained by interpolating from a finite set of diagnostic line-ratio grids computed with the MAPPINGS code. We used a

[14] http://fpavogt.github.io/pyqz/

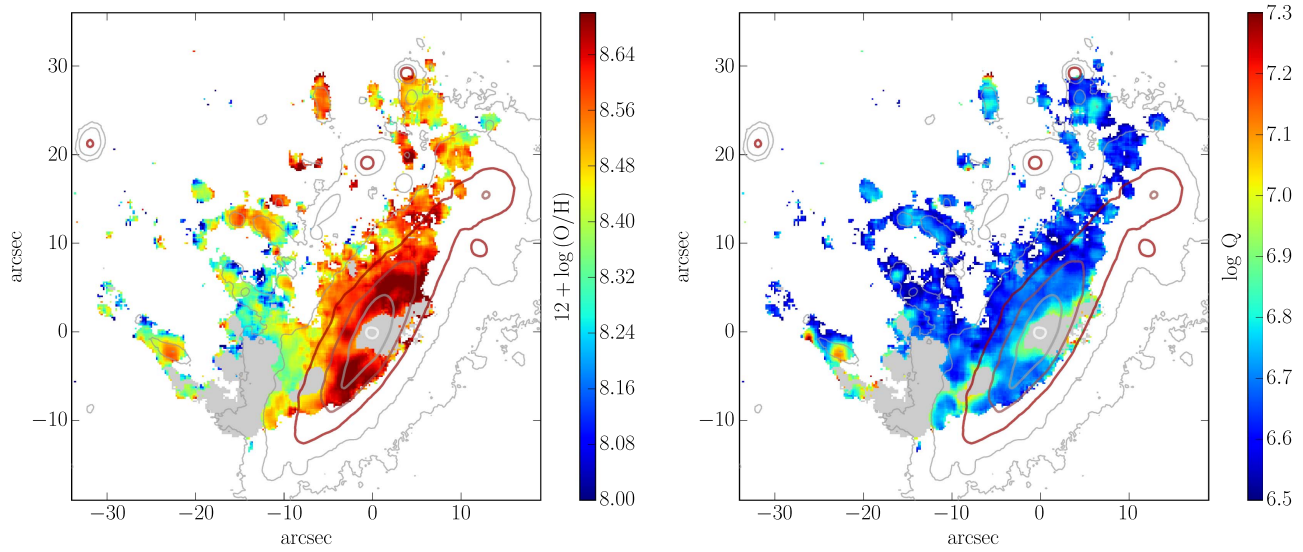

Figure 10. Metallicity (left panel) and ionization parameter (right panel) map. Regions ionized by LINERs/AGNs according to the BPT diagram have been masked (gray area). Contours are stellar isophotes, just as in Figure 4.

modified version of the code (F. Vogt 2017, private communication) to implement the MAPPING IV grids that are calibrated in the range $7.39 < 12 + \log(\mathrm{O/H}) < 9.39$, which is broader than the metallicity range covered by MAPPING V grids. Our results are based on the [N II]6585/[S II]6717+6731 versus [O III]/[S II]6717+6731 (see Poggianti et al. 2017b). The calibration applies only to star-forming regions, therefore we masked out all regions classified as AGNs or LINERs. The resulting metallicity and ionization parameter maps are shown in Figure 10. The metallicity of the ionized gas varies by ∼0.7 dex. The inner galaxy disk is more metal-rich than the outskirts and the stripped tail, as expected. Interestingly, the western side of the gas tail (at coordinates $X \sim 5'$, $Y \sim 10'$ in Figure 10) seems to be more metal-rich than the eastern side, as if it were stripped from the inner—and hence more metal-rich—regions of the galaxy disk. This would in turn be explained if the galaxy velocity vector were not exactly perpendicular to the galaxy disk, but it would be pointing south (in the direction of the negative y-axis in Figure 10).

This is the second paper based on the GASP survey in which we analyze the physical properties of the stripped gas in a jellyfish galaxy; the previous one presented data for JO206 from Poggianti et al. (2017b). Future papers will compare the properties of GASP galaxies and the ionized gas. We note, however, that with respect to JO206, the ionized gas in JO204 is generally more metal-rich; instead, both galaxies have very low-ionization parameters with $\log q < 7$, as shown in the right panel of Figure 10.

3.6. Hα Knots

The ionized gas in JO204 is very clumpy, and as in most GASP galaxies, it presents many bright star-forming knots in the galaxy disk in and the tail; using the procedure described in Poggianti et al. (2017b), we identified and measured the size and Hα flux of 111 individual Hα knots in JO204; our measurements provide reliable flux measurements, taking care of deblending the contributions from overlapping sources. KUBEVIZ was then run to measure the integrated emission fluxes of all knots. The nature of these blobs was determined on the basis of BPT diagrams, as those described in Section 3.4. Figure 11 shows that 92 of these knots are star-forming/composite regions. Excluding the central emission peak due to the AGN itself, all AGN-powered knots are found in the eastern region, which was already discussed in the previous sections. The presence of a large number of star-forming H II regions provides support to our conclusion, presented in the previous section, that most of the gas in JO204 is ionized by hot stars. H II regions formed in situ in the gas tail seem to be a common feature of most galaxies undergoing gas-stripping (Yagi et al. 2013; Fossati et al. 2016; Poggianti et al. 2017b); however, this contrasts with the case of NGC 4569, a jellyfish galaxy in the Virgo cluster: Boselli et al. (2016) found no star-forming H II region in it and therefore they speculate that the gas is mainly excited by mechanisms other than photoionization (shocks in the turbulent gas, magnetohydrodynamic waves, and heat conduction).

The lower right panel in Figure 11 shows that the metallicity of the blobs follows the metallicity distribution of the diffuse gas. The H II regions on the west side of the gas tail (up to $X \sim 10$, $Y \sim 15$) are more metal-rich ($12 + \log(\mathrm{O/H}) > 8.6$ than those on the east side; this could be due to the fact that these H II regions formed from gas stripped from the center of JO204 rather than from the outer disk; this in turn provides some indications that the ram-pressure-stripping is acting along a south–north direction, as already noted in Section 3.5. This would implicate that the vector of the motion of JO204 across the ICM points downward on our maps (south).

The ongoing SFR of each blob was calculated from the Hα absorption- and dust-corrected flux as in in Poggianti et al. (2017b), adopting Kennicutt's relation for a Chabrier IMF:

$$\mathrm{SFR} = 4.6 \times 10^{-42} L_{\mathrm{H}\alpha}. \quad (1)$$

The total SFR for the 92 star-forming regions is 1.4 $M_\odot$ yr^{-1}, and the distribution of SFRs for all blobs is shown in Figure 12.

To compute the gas mass of each star-forming region, we estimated the electron density from the Proxauf et al. (2014) relation; this is based on the $R = $ [S II]6717/[S II]6737 line ratio and is valid in the range $0.4 < R < 1.435$. We refer to Poggianti et al. (2017b) for a detailed description of the procedure. Fifty-one knots have [S II] line ratios within the

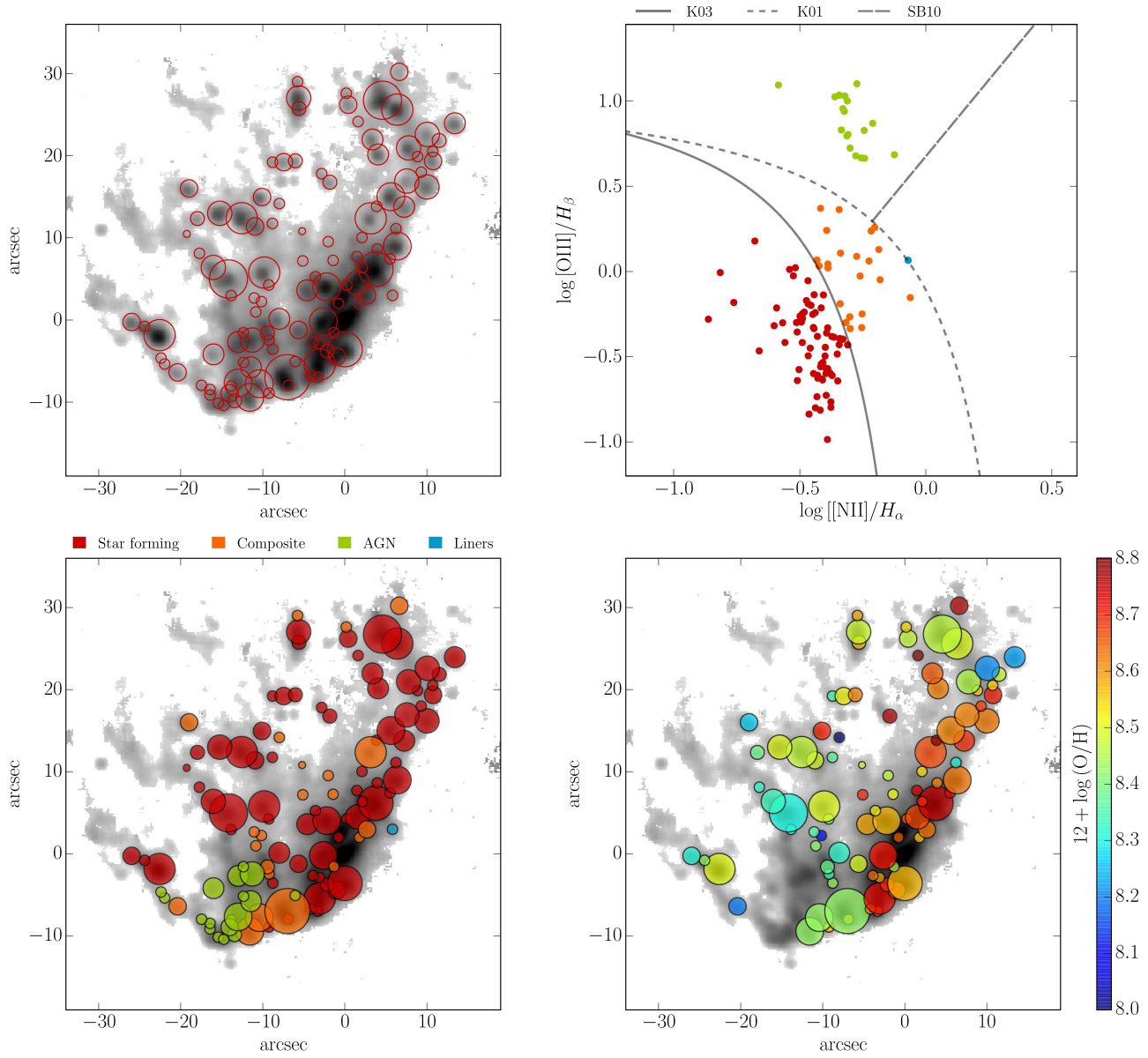

Figure 11. The upper left panel shows the 111 Hα knots detected in JO204. The location of each knot in the BPT diagram is shown in the upper right panel (the color-coding and lines are the same as in Figure 9) and it is used to derive the ionization mechanism; results are shown in the lower left panel. The metallicity of the 92 star-forming regions is shown in the lower right panel.

range where the density calibration applies. Their mass distribution is shown in Figure 12. The values we found range from 10^3 to $10^7\,M_\odot$ and the median value is $5.3 \times 10^4\,M_\odot$. The total gas mass of the 51 blobs is $1.8 \times 10^7\,M_\odot$. This is one order of magnitude lower than the total gas mass of the star-forming blobs in JO206 (Poggianti et al. 2017b). These results will be compared to those that are being obtained from other GASP galaxies to assess the general properties of star-forming regions in the stripped gas.

3.7. Star Formation History

An estimate of the total ongoing SFR can be obtained from the dust- and absorption-corrected Hα luminosity in the star-forming regions; toward this end, we integrated the Hα emission maps masking out all AGN- and LINER-powered regions (see Section 3.4) and found SFR $= 1.7\,M_\odot\,\mathrm{yr}^{-1}$. This is a hard lower limit to the total SFR because the AGN region accounts for about 45% of the total Hα luminosity. Our results, however, provide reliable estimates of the order of magnitude of the total SFR; using the results of the previous section, we can also conclude that—excluding AGN-powered regions—most of the star formation activity is taking place inside the compact H II regions. We also computed the total SFR outside the regions defined by the second, third, and fourth brightest stellar isophotes that are shown in all maps (e.g., Figure 5) and we found values of 1.5, 0.8, and $0.6\,M_\odot\,\mathrm{yr}^{-1}$, respectively; the SFR outside the main body of JO204 is therefore $\lesssim 0.5\,M_\odot\,\mathrm{yr}^{-1}$, which is much lower than the value found for JO206 ($\sim 1-2.5\,M_\odot\,\mathrm{yr}^{-1}$, Poggianti et al. 2017b); despite the spectacular tail of stripped gas and the large number of star-forming regions in the tail, at least two-thirds of the star formation activity in JO204 is taking place in the disk.

To estimate the total disk stellar mass, we integrated the spectra in the regions inside the three previously defined isophotes and ran SINOPSIS on the resulting spectra: the total

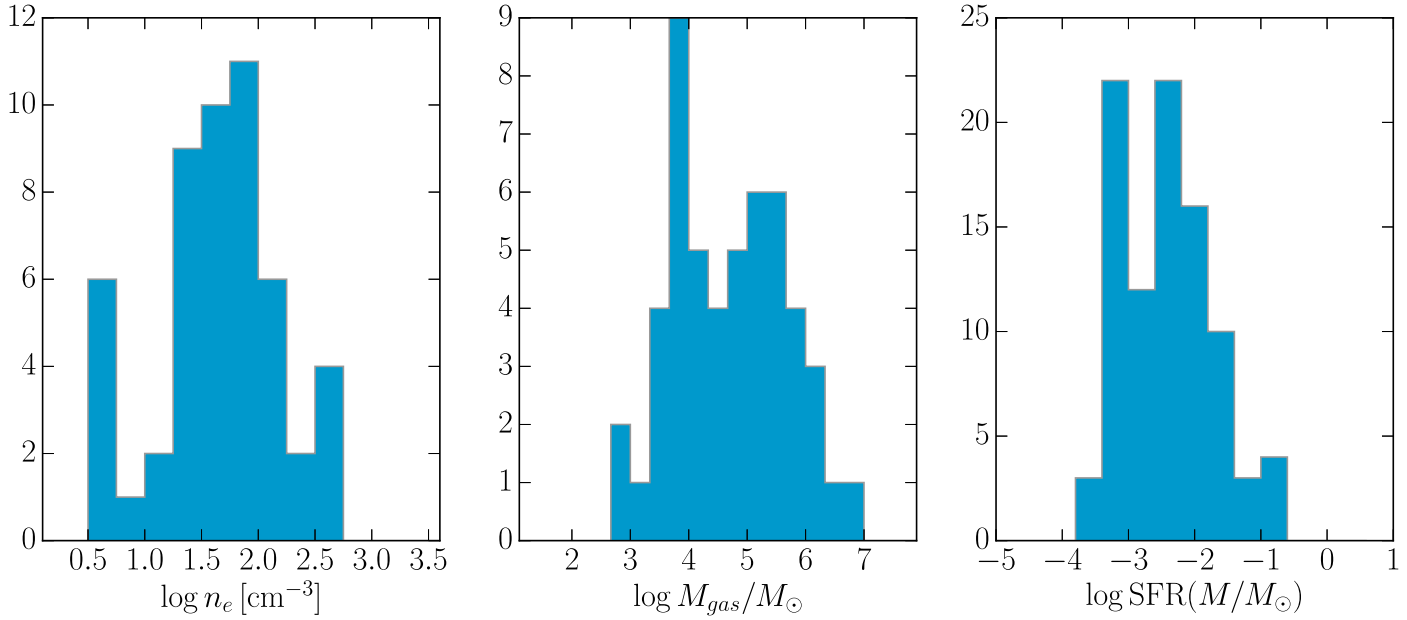

Figure 12. Distributions of gas density, mass, and SFR of individual Hα knots.

mass inside the inner isophote is $3 \times 10^{10}\,M_\odot$; inside the third isophote we computed a total mass of $4 \times 10^{10}\,M_\odot$ and found that the value inside the outer isophote is the same, within the uncertainties that are typically ∼10%–20%, showing that the stellar mass outside the outer isophote is negligible.

The spatially resolved star formation history of JO204 was reconstructed using the output of SINOPSIS. The results are shown in Figure 13. The ongoing star formation rate, as traced by stars born in the last 2×10^7 yr, is extremely intense in the inner disk, particularly in the very central region of JO204, as already discussed at the beginning of this section. We detected no ongoing star formation in the outer disk, where the gas has been already completely stripped and the star formation activity has been totally quenched. Some moderate ongoing star formation is detected everywhere across the stripped gas tail; the distribution is clumpy and the star formation activity is concentrated in the knots identified in the previous section.

The recent star formation (between 20 and 570 Myr, the second youngest age bin) is not distributed like the ongoing star formation (<20 Myr). It is rather intense in the outer disk and less peaked toward the center of the galaxy with respect to the ongoing star formation. Figure 13 suggests a modest presence of stars born in this age bin in the regions of the tail closer to the main body of the galaxy. Star formation activity in the external tail of JO204 is negligible between 20 and 570 Myr (Figure 13, upper left panel).

The distribution of the stellar populations older than 500 Myr is regular (see the two bottom panels in Figure 13, as expected for undisturbed disk galaxies. No old stellar population is detected in the tails of JO204.

The SFH in the outer disk is peaked within the second age bin; this is expected, as we have already shown that the spectra in these regions have post-starburst features, indicating vigorous star formation activity that was abruptly interrupted less than 1 Gyr ago. The oldest stars in the (inner) tails were born within the last ∼500 Myr; this should therefore be the epoch of the onset of the gas-stripping and the beginning of the gas tail. The burst of star formation in the outer disk should have therefore been induced by the compression due to ram-pressure in this region.

4. JO204 Environment

JO204 is a member of A957, a relatively low-mass cluster with an X-ray luminosity $L_X = 7.8 \times 10^{43}$ erg s^{-1} in the 0.1-2.4 keV band (Ebeling et al. 1996). From the analysis of OmegaWINGS spectroscopy, Moretti et al. (2017) measured a total cluster mass $M = 4.4 \times 10^{14}\,M_\odot$, a velocity dispersion $\sigma_v = 640$ km s^{-1}, a systemic cluster redshift $z = 0.0451$, and a size $R_{200} = 1.5$ Mpc. For JO204 we measured a systemic redshift $z = 0.04243$, therefore the galaxy moves with a radial velocity of -800 km s^{-1} with respect to A957, which corresponds to 1.25 times the cluster velocity dispersion. JO204 is located in the central region of the cluster, at a projected clustercentric distance of 2.′1, which corresponds to 132 kpc or 0.08 R_{200}.

The left panel of Figure 14 shows the location of JO204 within the cluster (star). Cluster members of A957 plotted as gray circles for reference, along with four galaxy groups identified by a substructure analysis (colored squares, Biviano et al. 2017, in preparation). Although several substructures are present in the cluster, JO204 is not associated with any of them. The right panel of Figure 14 further shows the location of JO204 in a projected clustercentric distance versus velocity phase–space diagram. In these kinds of plots, gravitationally bound galaxies congregate inside a trumpet-shaped region enclosed by the escape velocity (gray curves), with the majority of galaxies in the low r and low $|\Delta_v|$ region. The bulk of galaxies near the center were accreted a long time ago and thus can be thought of as virialized. The most recent members of the clusters, on the other hand, can be distributed across the whole diagram, and tend to have higher absolute velocities (and velocity dispersion) than the virialized population (see Haines et al. 2015; Jaffé et al. 2015, 2016).

Using the (projected) phase–space position of JO204, we can estimate the expected ram-pressure intensity exerted by the

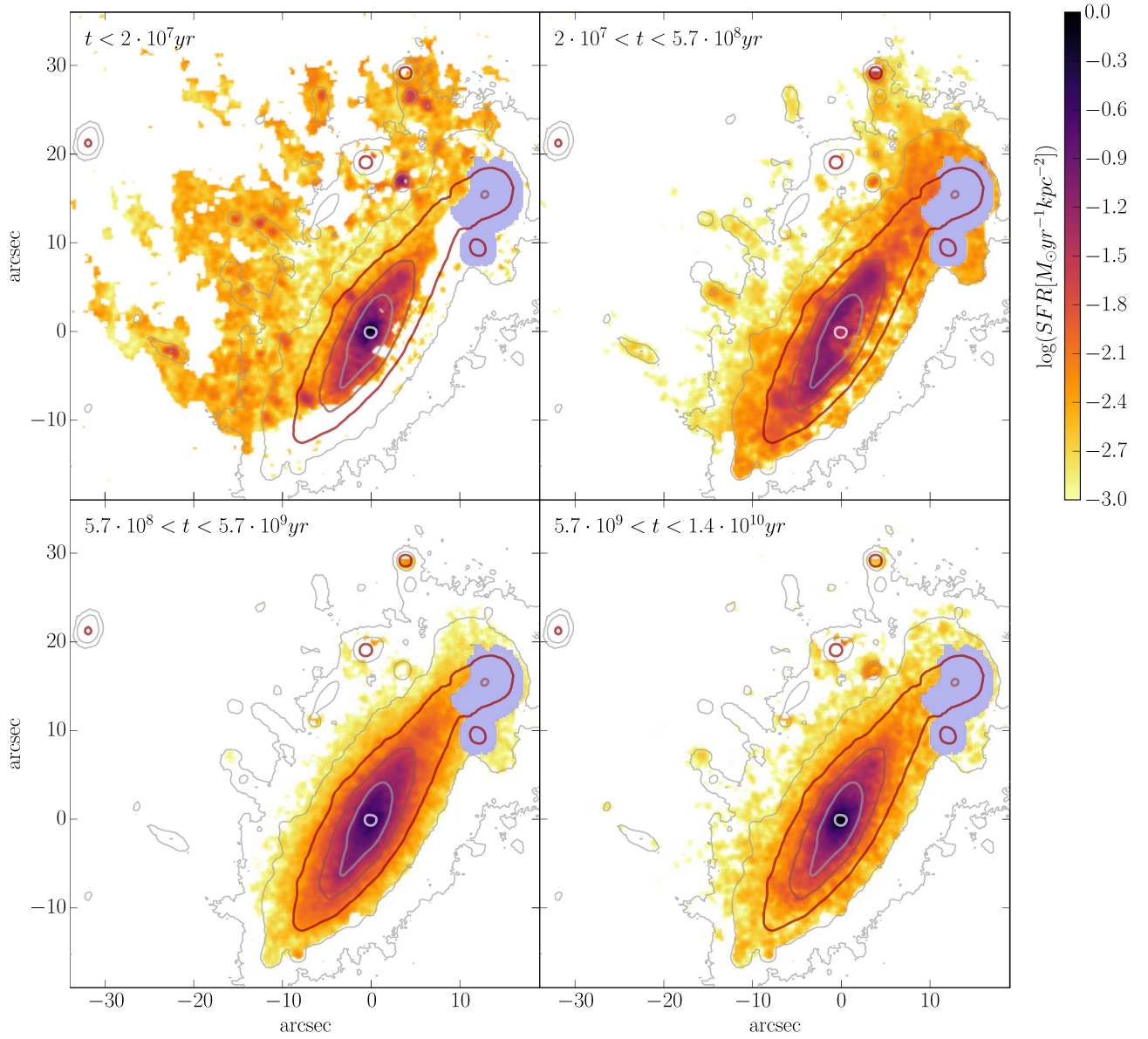

Figure 13. Maps of the average star formation rate per kpc^2 in four different age bins. The areas shaded in blue are regions contaminated by interloper galaxies; these were excluded from the SINOPSIS analysis because we could not define the redshift of either the gas or the stellar component. The contours show the Hα-continuum, just as in Figure 4.

cluster as

$$P_{\rm ram} = \rho_{\rm ICM} \times \Delta v_{\rm cl}^2 \quad (2)$$

(Gunn & Gott 1972), where $\rho_{\rm ICM}(r_{\rm cl})$ is the radial density profile of the ICM, $r_{\rm cl}$ is the clustercentric distance, and $\Delta v_{\rm cl}$ is the velocity of the galaxy with respect to the cluster. Since A957 is a low-mass cluster similar to the well-studied Virgo cluster, we adopt the ICM density values of Virgo from Vollmer et al. (2001) and obtain a value for the ram-pressure of $P_{\rm ram} = 4.2 \times 10^{-13}$ N m^{-2}. We note that this is a lower limit to $P_{\rm ram}$, as it is based on the projected distance and velocity of the galaxy with respect to the cluster. In particular, considering the extent of the galaxy tails in the sky, the projected velocity is likely an underestimation of the full velocity.

To test how much ram-pressure-stripping is caused on the disk of JO204, we compute the anchoring force of the galaxy assuming an exponential disk density profile for the stars and the gas components (Σ_g and Σ_s respectively) as:

$$\Sigma = \left(\frac{M_{\rm d}}{2\pi r_{\rm d}^2}\right) e^{-r/r_{\rm d}}, \quad (3)$$

where $M_{\rm d}$ is the disk mass, $r_{\rm d}$ is the disk scale-length, and r is the radial distance from the center of the galaxy. For the stellar component of JO204 we adopted a disk mass $M_{\rm d,\star} = 4 \times 10^{10} M_\odot$, and a disk scale-length $r_{\rm d,\star} = 4.2$ kpc, obtained by fitting the light profile of the galaxy. For the gas component we assumed a total mass $M_{\rm d,gas} = 0.15 \times M_{\rm d,\star}$ (Popping et al. 2014), and scale-length $r_{\rm d,gas} = 1.7 \times r_{\rm d,\star}$ (Boselli & Gavazzi 2006).

The above values can be used to compute the anchoring force in the disk at different r, following

$$\Pi_{\rm gal} = 2\pi G \Sigma_g \Sigma_s. \quad (4)$$

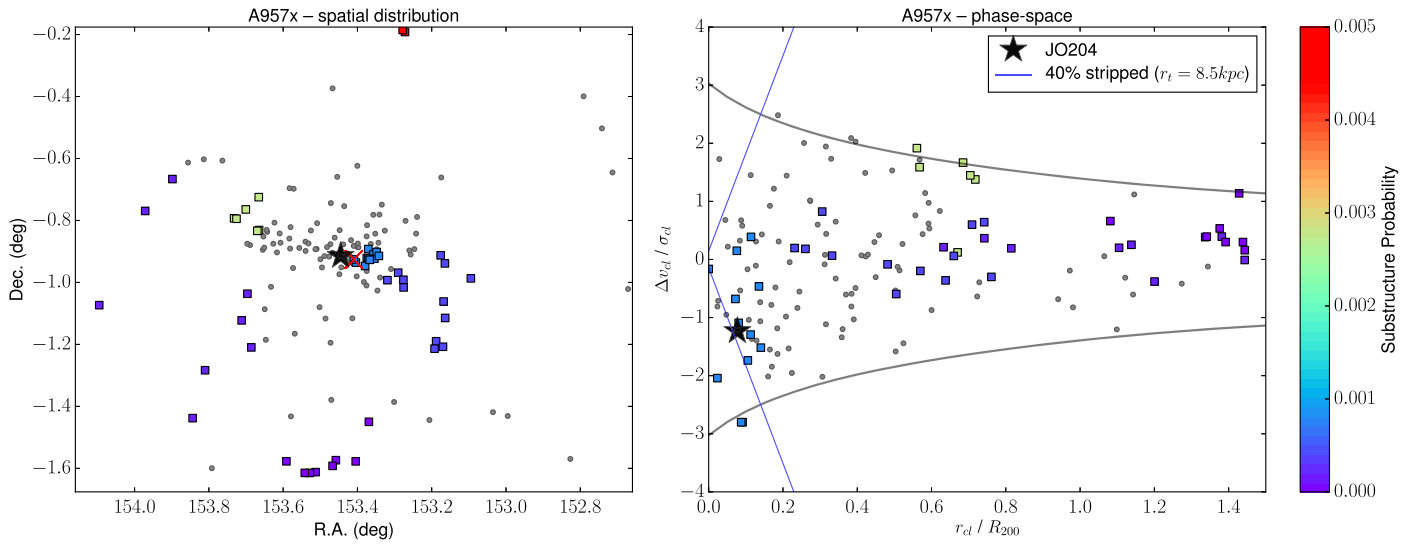

Figure 14. The position in the sky of the spectroscopic members of A957 from OmegaWINGS (small gray circles), JO204 (black star), and the BCG (red cross). Squares correspond to identified substructures, which have been color-coded according to their probability of being random fluctuations (i.e., values close to zero indicate highly significant substructure detections; Biviano et al. 2017, in preparation). Right: position vs. velocity phase–space diagram. The gray curves show the escape velocity in a Navarro et al. (1997) halo. The dashed lines intersecting with the position of JO204 correspond to 30% of the total gas mass stripped in JO204 by the ICM in a Virgo-like cluster (see the text for details). The solid blue line corresponds to the expected stripping from the extent of the (truncated) Hα emission (64% of the total gas mass stripped).

In the phase–space diagram of Figure 14 we plot several stripping lines, corresponding to different stripping (or truncation) radii, r_t. In each case, the fraction of remaining gas mass can be computed as

$$f = 1 + \left[e^{-r_t/r_d} \left(\frac{-r_t}{r_d} - 1 \right) \right]. \quad (5)$$

We find that the condition for stripping ($P_{ram} > \Pi_{gal}$) is met at a truncation radius of ~8.5 kpc (40% of the total gas mass stripped). This radius coincides remarkably well with the extent of the Hα emission with respect to the stellar disk.

Overall, our analysis suggests that the gas in JO204 is being significantly stripped by a ram-pressure force perpendicular to the disk.

5. Hydrodynamical *N*-body Simulations

To model JO204's evolution, we used the simulation code *GIZMO* (Hopkins 2015) in its "meshless finite-mass" implementation of the hydrodynamics-solver.

We followed Bischko et al. (2015) in modeling a constant ram-pressure in a wind-tunnel-like setup, acting on galaxy initial conditions generated to resemble the pre-interaction properties of JO204. The galaxy initial conditions generator is described in Springel et al. (2005). For JO204, these initial conditions are comprised of dark matter particles distributed in accordance with a Hernquist profile.[15] Concentrically embedded in this dark matter halo are exponential disks, one each for the stellar and gaseous components. These galaxy models are then pre-aged in isolation for one Gyr in order for star formation to self-regulate and the disks to stabilize before they can be placed in the wind tunnel.

The initial gas fraction f_{gas} of our models was estimated from the stellar mass using the relations in Popping et al. (2014), as in Section 4. We varied the remaining parameters of the halo and those of the ICM in a grid of simulations. The radial velocity of JO204 with respect to A957 served as a lower limit for the ICM velocity relative to the model galaxy ($|\Delta v_{ICM}| > |\Delta v_{cl}|$). Similarly, the clustercentric distance in the viewing plane was assumed as a lower limit for the three-dimensional distance of JO204 to A957. The latter was used to obtain limits for the simulated density of the ICM (ρ_{ICM}). We assumed a beta-profile[16] and used the parameters in Ebeling et al. (1996) and Abramopoulos & Ku (1983) for A957, giving us a rather large range of $\sim 2.2 \cdot 10^{-28}$ to $\sim 1.4 \cdot 10^{-27}$ g cm^{-3} for ρ_{ICM}. The initial parameters of the best-match simulation and the fit parameters of the stellar disk are listed in Table 1.

Table 1
Parameters of the Closest Matching Simulation in the Ensemble

Parameter	Symbol	Value	Unit
halo concentr.	c	12	...
halo circ. vel.	v_{200}	120	km s^{-1}
spin parameter	λ	9.5	%
stellar mass	$M_{d,\star}$	$4{\cdot}10^{10}$	$M_\odot$
gas mass	$M_{d,gas}$	$6{\cdot}10^{9}$	$M_\odot$
disc scalelen.	r_d	4.2	kpc
disk height	z_0	0.2	r_d
ICM density	ρ_{ICM}	$5{\cdot}10^{-28}$	g cm^{-3}
ICM vel.	$\lvert\Delta v_{ICM}\rvert$	1000	km s^{-1}
ICM incl.	β	30	deg
viewing angle	α	−18	deg

Note. First are the galaxy initial condition parameters, followed by the properties of the simulated ICM, and lastly, the viewing angle. Note that some parameters (particularly the disk scale-length) are subject to moderate change during pre-aging and simulation in the wind tunnel.

[15] Hernquist (1990) profile: $\rho_{dm}(r) = \frac{M_{dm}}{2\pi} \frac{a}{r(r+a)^3}$ with $a = r_s\sqrt{2[\ln(1+c) - c/(1+c)}$ and $c = r_{200}/r_s$, where r_s is the scale-length of a regular NFW halo (Navarro et al. 1997).

[16] Beta-profile: $\rho_{icm}(r) \approx \rho_0[1 + (r/r_c)^2]^{-3/2\beta}$, (Cavaliere & Fusco-Femiano 1978).

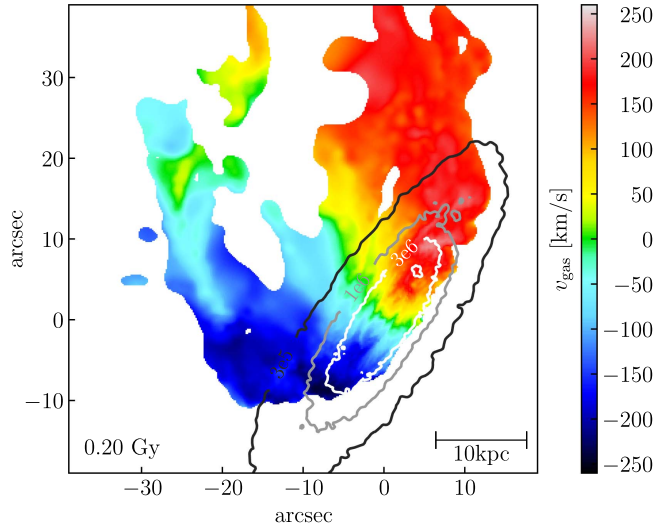

Figure 15. Velocity map of the closest-matched simulation in our grid. Superimposed are contours of equal stellar mass (per pixel).

Figure 15 shows the velocity field of our closest-matched simulation. To generate Figure 15, we interpolated the LOS-velocity of the simulated gas particles with a nearest-neighbor-based smoothing-kernel and integrated the resulting 3D map along the LOS (similar to Steinhauser et al. 2016). Pixels with a (LOS-integrated) gaseous mass below a threshold of $\sim 30\ M_{\odot}$ were removed. These pixels stem from sparse regions, where the particle density in the simulation is low. These pixels would otherwise lead to artifacts and inaccurate results at the outskirts of the gaseous wake in Figure 15.

The stripping fraction was estimated by engulfing the disk stars in a cylinder of a thickness equal to twice the disk height. The cylinder is centered on the disk stars. The stripping fraction is then taken as the mass ratio of the gas outside this cylinder, versus total gas mass:

$$f_{\rm strip} = \frac{M_{\rm gas,out}}{M_{\rm gas,cyl}} \sim 40\%.$$

This is in remarkable agreement with the fraction of stripped gas derived from analytical considerations (Section 4).

There is an overall agreement between the gas velocity map in Figure 15 of the simulated galaxy and the velocity map of the JO204 gas component in Figure 7; the hydrodynamic simulations also confirm the reliability of our conclusion that the onset epoch of ram-pressure stripping is a few hundred-million years ago.

6. Summary and Conclusions

In this paper we presented MUSE observations from the ESO Large Program GASP, a survey of candidate gas-stripping galaxies. This paper focused on JO204, a member of the relatively low-mass cluster A957. The total exposure time of our MUSE observations is 4050 s; the detection limit on the final reduced datacube is $F_{\rm H\alpha} \simeq 10^{-17.5}$ erg s^{-1} cm^{-2} arcsec^{-2} (S/N = 5).

We summarize the main results of this paper as follows.

1. MUSE data unveiled a prominent tail of ionized gas stripped from the main body of the galaxy; it has an extension of $\sim$30 kpc in the direction perpendicular to the major axis of JO204 and it is $\sim$45 kpc wide.
2. The spectra of the outer disk show no emission by ionized gas and strong Balmer-line absorption. These features are typical of post-starburst stellar populations, whose star formation activity has been rapidly quenched at some point $\lesssim$1 Gyr ago.
3. The kinematics of the stellar component does not reveal any significant sign of perturbation from regular disk rotation.
4. The kinematics of the gas in the disk follows the rotation of the stellar component; this rotation is also retained—with minor local perturbation—by the gas and the H II regions in the tail.
5. Apart from the AGN and its ionization cone, most of the gas is ionized by in situ star formation.
6. We identified 92 star-forming blobs in JO204, which account for most of the total $\sim 2\ M_{\odot}$ yr^{-1} ongoing star formation rate.
7. The ongoing SFR outside the main body of the galaxy is estimated to be $0.6\ M_{\odot}$ yr^{-1}.
8. The star formation activity in the tail began during the last 500 Myr; in the external regions of the tail we did not detect stars older than 2 10^7 yr.

The interpretation of these data was supported by an analysis of the phase–space diagram and basic ram-pressure-stripping prescriptions (Gunn & Gott 1972); we also found further support to the conclusions drawn from MUSE by comparing the observed gas kinematics with the results from a set of hydrodynamical simulations. We conclude that JO204 is at the first infall in A957, in a highly radial orbit; a few hundred-million years ago, ram-pressure started stripping gas. The consequent compression of the gas induced a burst of star formation in the disk; the gas was then rapidly and completely removed from the outer disk, quenching the star formation. Ram-pressure-stripping proceeded outside-in and it is still active; we estimate that 40% of JO204's total gas mass has been stripped so far. The gas removed from the galaxy's main body collapsed in star-forming regions throughout the gas tail; excluding the AGN-powered regions, we found that about a third of the ongoing star formation (excluding the AGN-powered regions) is taking place outside the main galaxy body; this is very similar to the fraction found in JO206 by Poggianti et al. (2017b).

This galaxy is at a similar stage of stripping as another of the spectacular jellyfish galaxies of GASP, JO201 (Bellhouse et al. 2017), but with the stripping being observed in the plane of the sky rather than along the line of sight.

MUSE observations provided valuable data for probing the ionized gas and the stellar populations of GASP galaxies, as shown in this paper; these observations triggered a number of follow-up programs to probe all the gas phases and to study the connection between gas-stripping and star formation activity. JO204 was selected as a target for GASP follow-up programs aimed at studying the molecular gas (APEX, Moretti et al. 2017, in preparation), atomic gas (JVLA), and X-ray gas (*Chandra*) in this galaxy.

We would like to thank the anonymous referee for helping improve the paper. This work is based on observations collected at the European Organisation for Astronomical Research in the southern hemisphere under ESO program 196.B-0578. This work made use of the KUBEVIZ software, which is publicly available at http://www.mpe.mpg.de/?dwilman/kubeviz. We warmly thank Matteo Fossati and Dave Wilman for their

invaluable help with KUBEVIZ, and Frederick Vogt for useful discussions and help with optimizing pyqz. We acknowledge financial support from PRIN-INAF 2014. J.F. aknowledges financial support from a UNAM-DGAPA-PAPIIT IA104015 grant, Mexico. This work was co-funded under the Marie Curie Actions of the European Commission (FP7-COFUND). B.V. acknowledges the support from an Australian Research Council Discovery Early Career Researcher Award (PD0028506).

Facilities: VLT (MUSE), VST (OmegaCAM), AAT (AAOmega).

Software: KUBEVIZ, ESOREX, SINOPSIS, CLOUDY, pyqz, IDL, Python.

ORCID iDs

Marco Gullieuszik https://orcid.org/0000-0002-7296-9780
Bianca M. Poggianti https://orcid.org/0000-0001-8751-8360
Alessia Moretti https://orcid.org/0000-0002-1688-482X
Jacopo Fritz https://orcid.org/0000-0002-7042-1965
Yara L. Jaffé https://orcid.org/0000-0003-2150-1130
Jan C. Bischko https://orcid.org/0000-0002-6030-532X
Callum Bellhouse https://orcid.org/0000-0002-6179-8007
Daniela Bettoni https://orcid.org/0000-0002-4158-6496
Benedetta Vulcani https://orcid.org/0000-0003-0980-1499
Mauro D'Onofrio https://orcid.org/0000-0001-6441-9044
Andrea Biviano https://orcid.org/0000-0002-0857-0732

References

Abramopoulos, F., & Ku, W. H.-M. 1983, ApJ, 271, 446
Bacon, R., Accardo, M., Adjali, L., et al. 2010, Proc. SPIE, 7735, 773508
Baldwin, J. A., Phillips, M. M., & Terlevich, R. 1981, PASP, 93, 5
Barnes, J. E., & Hernquist, L. 1992, ARA&A, 30, 705
Bellhouse, C., Jaffé, Y. L., Hau, G. K. T., et al. 2017, ApJ, 844, 49
Bischko, J. C., Steinhauser, D., & Schindler, S. 2015, A&A, 576, A76
Boselli, A., Cuillandre, J. C., Fossati, M., et al. 2016, A&A, 587, A68
Boselli, A., & Gavazzi, G. 2006, PASP, 118, 517
Byrd, G., & Valtonen, M. 1990, ApJ, 350, 89
Calvi, R., Poggianti, B. M., & Vulcani, B. 2011, MNRAS, 416, 727
Cappellari, M., & Copin, Y. 2003, MNRAS, 342, 345
Cappellari, M., & Emsellem, E. 2004, PASP, 116, 138
Cardelli, J. A., Clayton, G. C., & Mathis, J. S. 1989, ApJ, 345, 245
Cavaliere, A., & Fusco-Femiano, R. 1978, A&A, 70, 677
Chabrier, G. 2003, PASP, 115, 763
Cortese, L., Marcillac, D., Richard, J., et al. 2007, MNRAS, 376, 157
Couch, W. J., & Sharples, R. M. 1987, MNRAS, 229, 423
Cowie, L. L., & Songaila, A. 1977, Natur, 266, 501
Dopita, M. A., Sutherland, R. S., Nicholls, D. C., Kewley, L. J., & Vogt, F. P. A. 2013, ApJS, 208, 10
Dressler, A. 1980, ApJ, 236, 351
Ebeling, H., Stephenson, L. N., & Edge, A. C. 2014, ApJL, 781, L40
Ebeling, H., Voges, W., Bohringer, H., et al. 1996, MNRAS, 281, 799
Fasano, G., Marmo, C., Varela, J., et al. 2006, A&A, 445, 805
Fasano, G., Poggianti, B. M., Bettoni, D., et al. 2015, MNRAS, 449, 3927
Fossati, M., Fumagalli, M., Boselli, A., et al. 2016, MNRAS, 455, 2028
Fritz, J., Moretti, A., Poggianti, B., et al. 2017, ApJ, submitted (arXiv:1704.05088)
Fritz, J., Poggianti, B. M., Bettoni, D., et al. 2007, A&A, 470, 137
Fritz, J., Poggianti, B. M., Cava, A., et al. 2011, A&A, 526, A45
Fumagalli, M., Fossati, M., Hau, G. K. T., et al. 2014, MNRAS, 445, 4335
Gavazzi, G. 1989, ApJ, 346, 59
Giovanelli, R., & Haynes, M. P. 1985, ApJ, 292, 404
Gullieuszik, M., Poggianti, B., Fasano, G., et al. 2015, A&A, 581, A41
Gunn, J. E., & Gott, J. R., III 1972, ApJ, 176, 1
Haines, C. P., Pereira, M. J., Smith, G. P., et al. 2015, ApJ, 806, 101
Hernquist, L. 1990, ApJ, 356, 359
Hopkins, P. F. 2015, MNRAS, 450, 53
Jaffé, Y. L., Smith, R., Candlish, G. N., et al. 2015, MNRAS, 448, 1715
Jaffé, Y. L., Verheijen, M. A. W., Haines, C. P., et al. 2016, MNRAS, 461, 1202
Kauffmann, G., Heckman, T. M., Tremonti, C., et al. 2003, MNRAS, 346, 1055
Kewley, L. J., Dopita, M. A., Sutherland, R. S., Heisler, C. A., & Trevena, J. 2001, ApJ, 556, 121
Kewley, L. J., Groves, B., Kauffmann, G., & Heckman, T. 2006, MNRAS, 372, 961
Larson, R. B., Tinsley, B. M., & Caldwell, C. N. 1980, ApJ, 237, 692
McPartland, C., Ebeling, H., Roediger, E., & Blumenthal, K. 2016, MNRAS, 455, 2994
Moore, B., Katz, N., Lake, G., Dressler, A., & Oemler, A. 1996, Natur, 379, 613
Moretti, A., Gullieuszik, M., Poggianti, B., et al. 2017, A&A, 599, A81
Moretti, A., Poggianti, B. M., Fasano, G., et al. 2014, A&A, 564, A138
Müller-Sánchez, F., Comerford, J. M., Nevin, R., et al. 2015, ApJ, 813, 103
Navarro, J. F., Frenk, C. S., & White, S. D. M. 1997, ApJ, 490, 493
Nulsen, P. E. J. 1982, MNRAS, 198, 1007
Owers, M. S., Couch, W. J., Nulsen, P. E. J., & Randall, S. W. 2012, ApJL, 750, L23
Peng, Y.-J., Lilly, S. J., Kovač, K., et al. 2010, ApJ, 721, 193
Poggianti, B. M., Fasano, G., Omizzolo, A., et al. 2016, AJ, 151, 78
Poggianti, B. M., Jaffe, Y. L., Moretti, A., et al. 2017a, Natur, 548, 304
Poggianti, B. M., Moretti, A., Gullieuszik, M., et al. 2017b, ApJ, 844, 48
Poggianti, B. M., Smail, I., Dressler, A., et al. 1999, ApJ, 518, 576
Popping, G., Somerville, R. S., & Trager, S. C. 2014, MNRAS, 442, 2398
Proxauf, B., Öttl, S., & Kimeswenger, S. 2014, A&A, 561, A10
Schlafly, E. F., & Finkbeiner, D. P. 2011, ApJ, 737, 103
Sharp, R. G., & Bland-Hawthorn, J. 2010, ApJ, 711, 818
Smith, R. J., Lucey, J. R., Hammer, D., et al. 2010, MNRAS, 408, 1417
Springel, V., Di Matteo, T., & Hernquist, L. 2005, MNRAS, 361, 776
Steinhauser, D., Schindler, S., & Springel, V. 2016, A&A, 591, A51
Véron-Cetty, M.-P., & Véron, P. 2010, A&A, 518, A10
Vollmer, B., Cayatte, V., Balkowski, C., & Duschl, W. J. 2001, ApJ, 561, 708
Wang, J.-M., Chen, Y.-M., Hu, C., et al. 2009, ApJL, 705, L76
Yagi, M., Gu, L., Fujita, Y., et al. 2013, ApJ, 778, 91

The Astrophysical Journal, 853:199 (2pp), 2018 February 1 https://doi.org/10.3847/1538-4357/aaa9bd
© 2018. The American Astronomical Society. All rights reserved.

Erratum: "GASP .IV. A Muse View of Extreme Ram-pressure Stripping in the Plane of the Sky: The Case of Jellyfish Galaxy JO204" (2017, ApJ, 846, 27)

Marco Gullieuszik[1], Bianca M. Poggianti[1], Alessia Moretti[1], Jacopo Fritz[2], Yara L. Jaffé[3], George Hau[3], Jan C. Bischko[4], Callum Bellhouse[3], Daniela Bettoni[1], Giovanni Fasano[1], Benedetta Vulcani[1,5], Mauro D'Onofrio[6], and Andrea Biviano[7]
[1] INAF, Astronomical Observatory of Padova, vicolo dell'Osservatorio 5, I-35122 Padova, Italy; marco.gullieuszik@oapd.inaf.it
[2] Instituto de Radioastronomía y Astrofísica, IRyA, UNAM, Campus Morelia, A.P. 3-72, C.P. 58089, Mexico
[3] European Southern Observatory, Alonso de Córdova 3107, Santiago, Chile
[4] Institute of Astro- and Particle Physics, University of Innsbruck, Technikerstrasse 25, A-6020 Innsbruck, Austria
[5] School of Physics, University of Melbourne, VIC 3010, Australia
[6] Department of Physics and Astronomy, University of Padova, Vicolo Osservatorio 3, I-35122 Padova, Italy
[7] INAF, Astronomical Observatory of Trieste, via G.B. Tiepolo 11, I-34131 Trieste, Italy
Received 2018 January 18; published 2018 February 5

We found a bug in the procedure we used to calculate the metallicity and ionization parameter that leads to estimates of both quantities that are smaller than the correct values. However, the main results and conclusions of the paper are neither based on the absolute value of the metallicity nor the ionization parameter; consequently, we do not need to amend any section of the paper. We just update Figures 1 and 2 (Figures 10 and 11 in the original paper) with the corrected values.

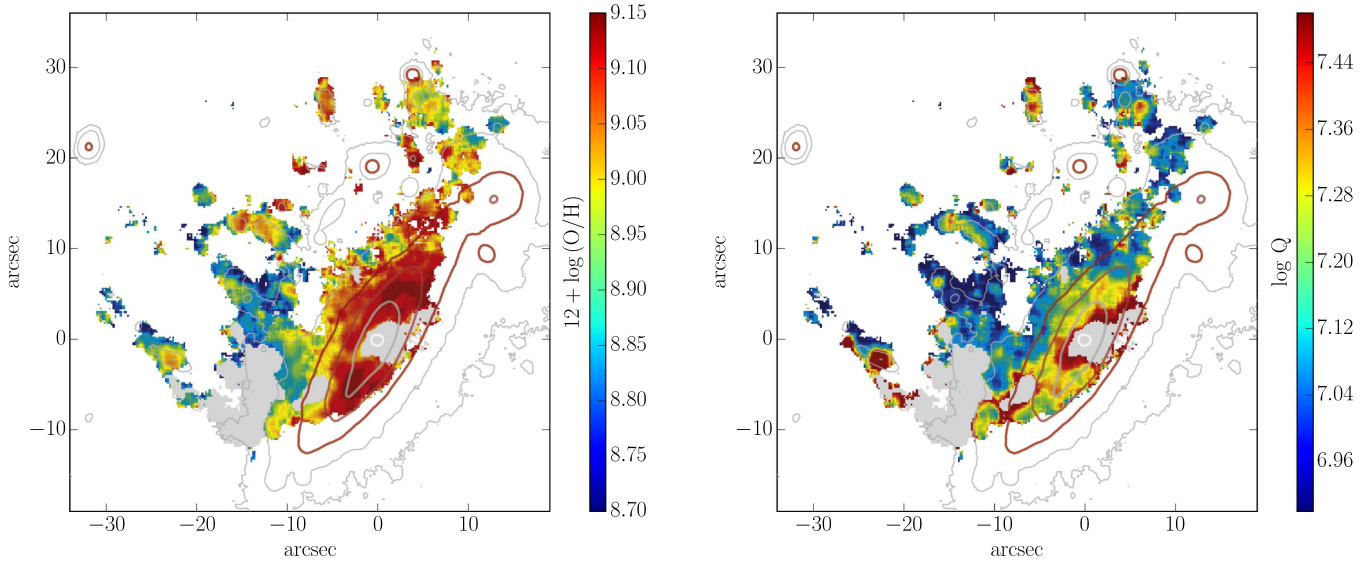

Figure 1. Figure 10 in the original paper. Metallicity (left panel) and ionization parameter (right panel) map. Regions ionized by LINERs/AGNs according to the BPT diagram have been masked (gray area). Contours are stellar isophotes, just as in Figure 4 in Gullieuszik et al. (2017).

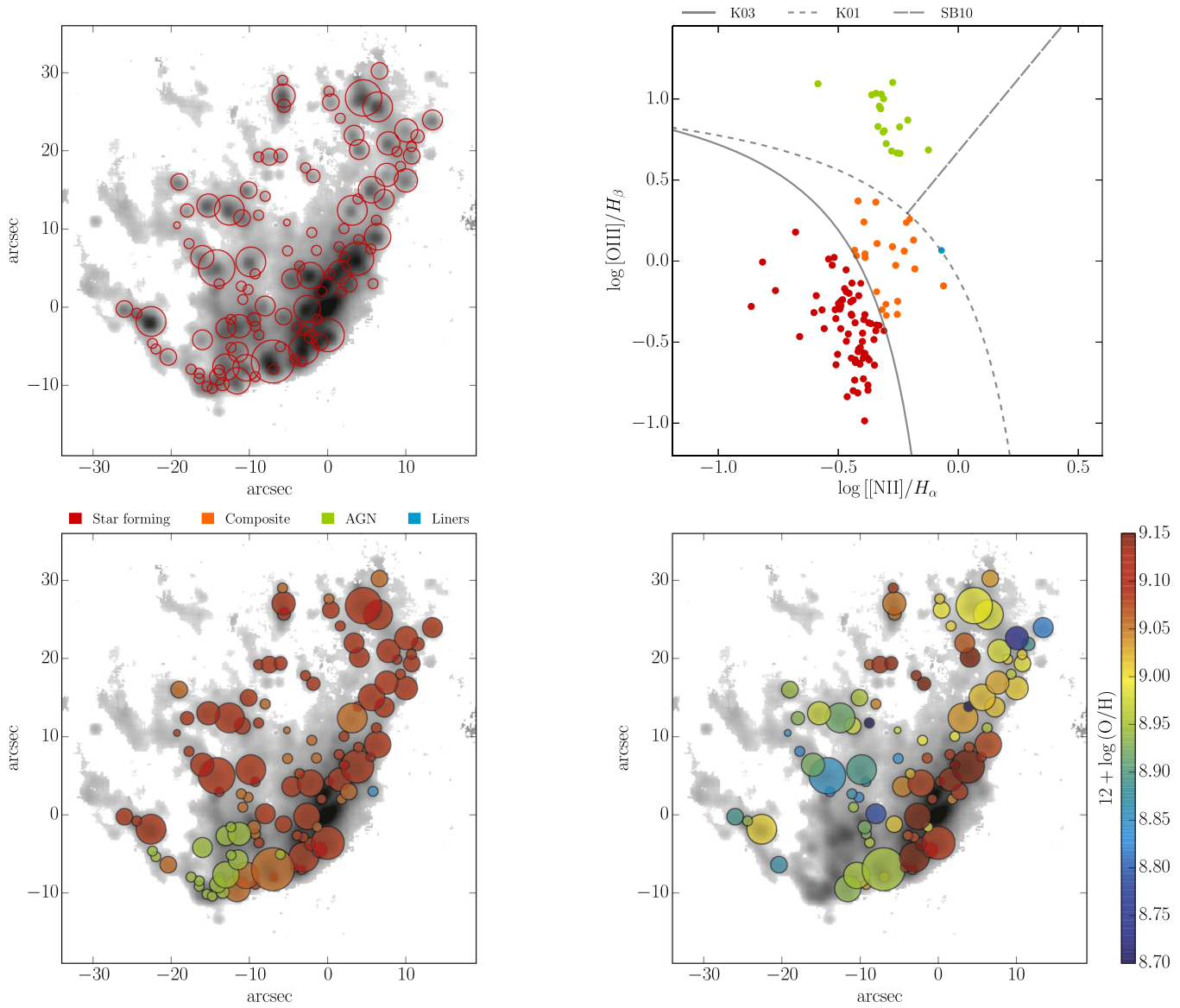

Figure 2. Figure 11 in the original paper. The upper left panel shows the 111 $H\alpha$ knots detected in JO204. The location of each knot in the Baldwin–Phillips–Terlevich diagram is shown in the upper right panel (the color-coding and lines are the same as in Figure 9 in Gullieuszik et al. 2017) and it is used to derive the ionization mechanism; results are shown in the lower left panel. The metallicity of the 92 star-forming regions is shown in the lower right panel.

ORCID iDs

Marco Gullieuszik https://orcid.org/0000-0002-7296-9780
Bianca M. Poggianti https://orcid.org/0000-0001-8751-8360
Alessia Moretti https://orcid.org/0000-0002-1688-482X
Jacopo Fritz https://orcid.org/0000-0002-7042-1965
Jan C. Bischko https://orcid.org/0000-0002-6030-532X
Callum Bellhouse https://orcid.org/0000-0002-6179-8007
Daniela Bettoni https://orcid.org/0000-0002-4158-6496
Benedetta Vulcani https://orcid.org/0000-0003-0980-1499
Mauro D'Onofrio https://orcid.org/0000-0001-6441-9044
Andrea Biviano https://orcid.org/0000-0002-0857-0732

Reference

Gullieuszik, M., Poggianti, B. M., Moretti, A., et al. 2017, ApJ, 846, 27